

Department of Atmospheric Sciences, University of Wyoming, Laramie, WY, USA

## Empirical estimation of the monthly-mean daily temperature range

B. Geerts

With 17 Figures

Received March 6, 2002; revised September 20, 2002; accepted November 3, 2002  
Published online ● ● ● © Springer-Verlag 2002

### Summary

This is a sequel to a study of the empirical estimation of the annual mean temperature and its range, at any location on land, based on the historical surface climate record. Here the spatial patterns of the daily temperature range (DTR) and its seasonal variation are examined. The DTR is highest in the subtropical deserts and is less at high latitudes, as well as within 30–150 km from an ocean. It is generally higher in winter (summer) at low (high) latitudes. The coastal DTR reduction is explained by sea breezes, onshore advection, and low-level cloud cover. Even large bodies of water, such as Lake Michigan, affect the near-shore DTR. Elevation does not directly affect the DTR, but valleys tend to have a DTR that is 2–6 K larger than adjacent hills or ridges.

The main factor affecting the DTR is the afternoon relative humidity, which is dynamically linked to low-level cloud cover. An empirical relationship between DTR and afternoon relative humidity has an uncertainty of about 1.4 K for monthly-mean values.

### 1. Introduction

This is a sequel to studies of the empirical estimation of the *annual mean* temperature (Linacre and Geerts, 2002, referred to as LG02) and the *annual range* of temperature (Geerts, 2002a) at any location on land, using only geographical information – latitude, elevation, and distance from the ocean shore at the same latitude. In these studies climatological surface temperature

distributions on land were analysed in order to shed light on the dominant physical processes, and to quantify their effects. Here the same global datasets of weather station records and gridded re-analysis are used to deduce climatological patterns of *daily range* of temperature, and its seasonal variation. The daily (or diurnal) temperature range (DTR) for a month is defined as the long-term mean of the daily difference between the maximum and minimum surface-air temperature for that month. These temperatures are obtained from the readings of a min/max thermometer or from hourly observations. Such DTR values represent the true amplitude, not the periodic one resulting from twice-daily measurements (Crowe, 1971, p. 64).

The diurnal temperature cycle is important for agriculture and natural ecosystems, perhaps as important as the mean temperature itself. It has received a great deal of attention in recent years as the historical climate-station record indicates that it has changed (Karl et al., 1993). A decrease in DTR has been observed in most regions of the world. This decrease globally averages 0.4 K between 1950–1993 (Easterling et al., 1997). A DTR decrease is consistent with increased urbanization during the past century (Kukla et al., 1986), but it has been observed for rural stations

as well (Gallo et al., 1999). This decrease is believed to be due largely to an increase in water vapour and low-level cloudiness (Easterling et al., 1997; Dessens and Bücher, 1995). The observed changes and their interpretation have been confirmed by means of general circulation model simulations (e.g. Hansen et al., 1995; Mearns et al., 1995; Watterson, 1997).

In order to gain an insight into these observed and predicted *changes* in DTR, it is important to understand the processes that explain the regional and seasonal variations of the *climatological* DTR. The present study uses climatological DTR data to illustrate and interpret spatial and seasonal DTR variations, and establishes and tests empirical relationships between basic geographic patterns and the DTR. The main data sources for this study are a) the International Station Meteorological Climate Summary, version 4.0, issued on a CD-ROM by the US National Climate Data Center in 1996 (referred to as ISMCS), and b) the NCAR/NCEP global re-analysis of weather station, buoy and satellite data between 1968–96 (Kalnay et al., 1996) (referred to as NNGR), accessed at <http://www.cdc.noaa.gov/>. The NNGR spatial resolution is 2.5 degrees. Other data sources include Linacre (1992), hereafter referred to as L92, and Linacre and Geerts (1997), i.e. LG97.

A global perspective (Section 2) demonstrates how latitude and distance from the ocean affects the daily range. After examining these two factors in Sections 3 and 4, respectively, the relationship between DTR and low-level cloudiness and its proxies is explored in Section 5. In Section 6 it is shown that elevation does not directly influence DTR, and that a physically meaningful relationship exists between terrain shape and DTR. Finally, the accuracy of a simple empirical relationship between DTR and afternoon relative humidity is assessed.

## 2. The daily range from a global perspective

The annual-mean value of the DTR between 65° N–65° S is shown in Fig. 1. According to this figure, the following factors govern the large-scale variation of DTR:

- *Land vs. sea.* The main contrast in Fig. 1 is that between land and ocean. The DTR is less

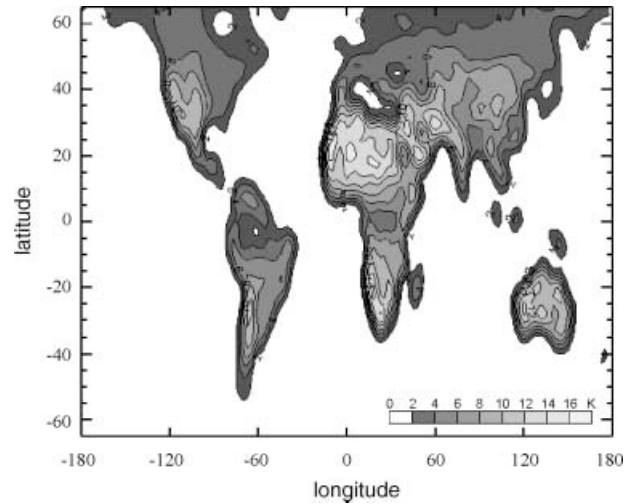


**Fig. 1.** Global distribution of the annual-mean DTR between 65° N–65° S, based on the NNGR surface temperature data. The contour interval is 2 K. The coastlines are not shown

than 2 K over oceans. In the absence of synoptic changes, the air temperature over sea varies little from day to night, because the sea surface temperature is nearly constant (Deacon, 1969, p. 84). A large coastal gradient exists, whilst DTR values become more uniform inland. Inland seas, such as the Mediterranean, have a significant effect on the DTR. The width of the littoral belt and the effect of smaller seas cannot be assessed from the NNGR data, given their coarse resolution (2.5°).

- *Latitude.* The DTR generally decreases from the Tropics towards 65°. This reflects the fact that the amplitude of the annual-mean diurnal cycle of the top-of-the-atmosphere solar radiance is largest at the equator and decreases poleward, at a rate proportional to the sine of latitude. The DTR has less meaning poleward of the polar circle (66.5°), where the Sun fails to set or rise for days to months. At such latitudes the DTR relates less to the surface energy balance and more to synoptic (interdiurnal) variations. But the DTR over land is *smaller* near the equator than around 20–30° latitude (Fig. 1), suggesting another important influence on DTR, i.e. cloudiness.
- *Cloudiness.* The highest DTR is found in the Sahara, where low clouds are rare, whilst the DTR is generally less than 6 K in Europe, where low clouds are common. The DTR on land is largely controlled by the amplitude of

the diurnal cycle of net radiation at the surface. This amplitude is less under cloud cover. Clouds, especially low clouds, reduce the incoming solar radiation and the nocturnal radiation deficit at the Earth surface (LG97 p. 66–67). Clear skies are common near the Tropics, especially in winter.

Other determinants of DTR, such as terrain shape and prevailing wind speed, are too local to be apparent in Fig. 1. The DTR may further be influenced by land surface conditions affecting the surface energy balance, such as albedo, roughness, and soil moisture content. In fact the DTR tends to be lower in cities than in the surrounding rural areas (Landsberg, 1981; Gallo et al., 1996), and lower over large irrigated croplands than in the adjacent arid environment (Dai et al., 1999; Geerts, 2002b). These influences, whose magnitude is on the order of 1 K, are beyond the scope of this study. Here we will focus on terrain effects and the three factors listed above.

### 3. Latitude

One might expect the DTR to decrease from the latitude of zenithal Sun towards the poles, as the daily maximum elevation of the Sun decreases, and therefore the amplitude of the daily cycle of net radiation at the surface decreases. But Fig. 2 shows that the zonal-mean annual-average DTR, over both continents and oceans, is low near the equator and peaks at 20–40° N and at 20–30° S. The fraction of land in each latitude belt clearly

dominates this variation and explains the difference in DTR between hemispheres.

The annual-mean DTR within the Tropics generally exceeds the annual range (Geerts 2002a, Fig. 1). This also applies in some coastal areas further poleward, such as the northern California coast around 40° N. Figure 2 also shows that the DTR within the Tropics is higher in winter, even though at noon the Sun is lower in the sky than in summer. The reason is that rainfall and cloudiness are more common at high Sun at low latitudes. These imply a lower DTR, as will be shown in Section 5.

The latitudinal variation of DTR at inland stations (inland of the coastal influence, discussed in Section 4) is more symmetric across the equator than that of the zonal-mean DTR. Minima occur near the equator and at high latitudes. The DTR maximum occurs near 35° in summer (Fig. 3a) and near 20° in winter (Fig. 3b). The variation again reflects the effect of cloudiness more than that of extraterrestrial radiation, as shown in Section 5. The DTR is about 5 K larger in winter than in summer at 15–20°, due to the seasonal movement of the zenithal rain belt. Low-level cloud cover also explains the difference in DTR between the western Americas and Europe/Africa between 15–50° N in Fig. 3a.

Poleward of 30° the DTR is largest in summer (Fig. 3; LG97, p. 55), when daytime solar radiation is stronger than in winter, causing more warming. Also, summertime longwave radiation loss at night is greater, as the surface temperature is higher. And summers in the mid-latitude belt usually bring more clear skies and weaker winds,

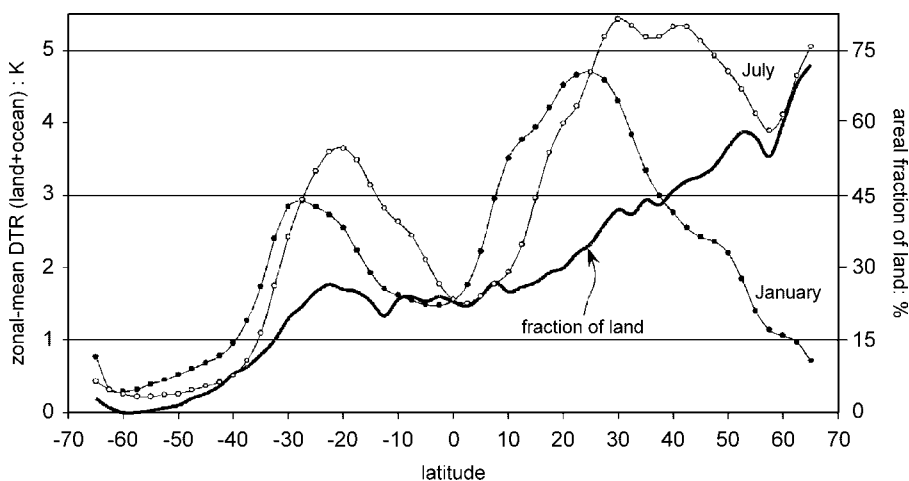


**Fig. 2.** Variation with latitude of the zonal-mean DTR for July (open circles) and January (solid circles), based on gridded NNGR surface-air temperatures. Also shown is the percent of land surface (bold solid line)

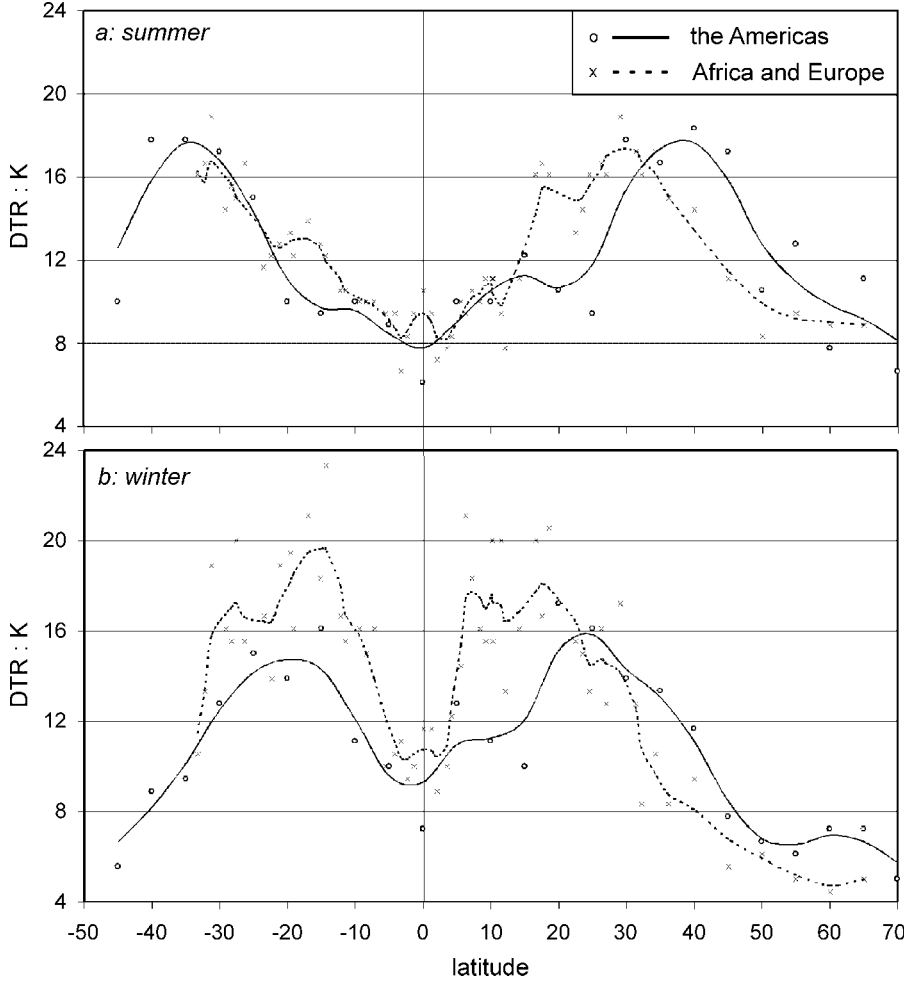


**Fig. 3.** The effect of latitude on the DTR (a) in summer [i.e. July (January) in the northern (southern) hemisphere], and (b) in winter (ISMCS data). All stations are located between 75–200 km inland from the west coast. A 5-point filter, applied to observations in the Americas (Africa & Europe), is shown by a solid (dashed) line

both of which enhance the DTR. As a result, the July DTR, compared to the January DTR, is about 5 K larger in Europe and 6–12 K larger in the western USA at 46° N. The DTR is only about 2 K larger in January than in July around 30° S in Australia, beyond the strip near the ocean where sea breezes and cloudiness suppress the daily maxima in summer. The seasonal difference in DTR increases with latitude, because of the enhanced ratio of summer to winter radiance at the top of the atmosphere. That ratio is 1.7 at local solar noon at 30° N, but 2.5 at 45° N and 7.1 at 60° N (LG97, Note 2.F).

The following relationships between DTR and latitude  $L$  (degrees, positive in both hemispheres) are the best match to the data in Fig. 3, ignoring the differences between the Americas and Africa & Europe. The terms  $R_{ds}$  and  $R_{dw}$  (K) refer to the DTR in the peak summer and winter months respectively, i.e. July or January.

$$R_{ds} = 12.34 - 3.80 \cos(\pi L/35) \quad (1a)$$

$$R_{dw} = 14.31 - 3.41 \cos(\pi L/20) \quad (|L| < 40^\circ) \quad (1b)$$

$$R_{dw} = 12.8 - 0.114 L \quad (|L| > 40^\circ) \quad (1c)$$

According to Eq. 1, the DTR is reduced near the equator, peaks near the Tropics (20° in winter and 35° in summer), and decreases poleward from there. The mean absolute error of the DTR estimated using Eq. 1 is 0.9 K in summer and 1.5 K in winter, for the DTR observations shown in Fig. 3. While the amplitude of this latitudinal variation is significant, Eq. 1 should not be used to “remove” the effect of latitude [a technique used in previous studies to focus on other factors affecting temperature variations (LG02, Geerts 2002a)], because zonal variations of DTR are at least as large as the meridional one (Fig. 1).

#### 4. Distance inland

##### 4.1 Observations

Some transects of observed DTR versus distance to the nearest shore are now examined, to answer the question – how does the DTR change across the coastal fringe? (The term ‘fringe’ does not correspond with the same term in LG02, where it is a belt of littoral warming along most west coasts). The DTR is steady in Australia’s interior but dwindles towards the east coast, from about 50 km inland in winter and 150 km in summer (Fig. 4). This is confirmed by transects at 19° S and 29° S across Australia (L92, p. 82). On the other hand, the dependence of DTR on distance inland near the coast in France is weak (in summer) or insignificant (in winter). This is because

in France the diurnal cycle of solar forcing is weaker, cloudy skies are more common, and onshore winds more persistent and stronger.

Inland seas and large lakes also affect the DTR, at least in summer. Figure 5 shows the variation of DTR east of Lake Michigan and east of the Black Sea. These water bodies are about 130 km and 1000 km wide, respectively. Westerly winds prevail at both places, of about the same latitude, at least in the winter. The July DTR is depressed by 2–3 K along the eastern shore of Lake Michigan, and by 3–4 K along the eastern shore of the Black Sea. The DTR reduction occurs within 20 km from the shore, i.e. not as far as from the Australian coast (Fig. 4). The prevailing wind direction appears to be of little significance. On the west side of Lake Michigan,

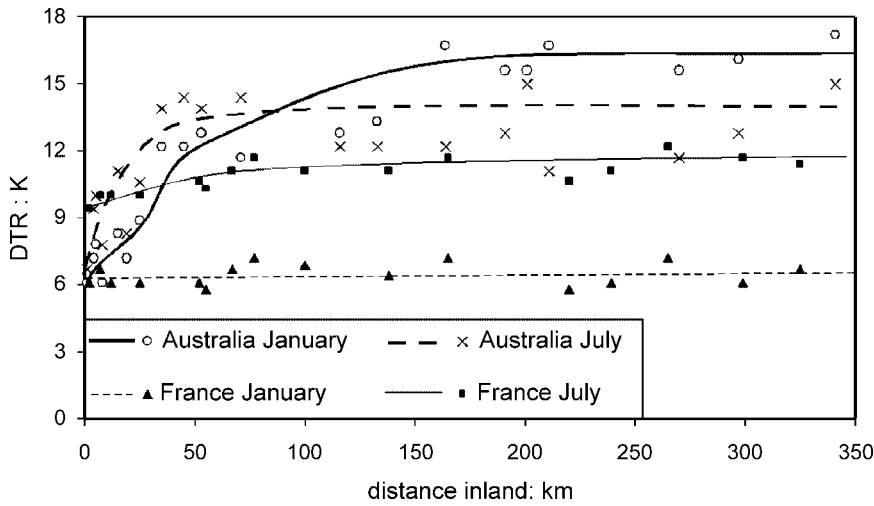


**Fig. 4.** Effect of distance to the nearest shore on the DTR in January and in July at stations between 27–34° S in Australia, and between 44–47° N in France (ISMCS data)

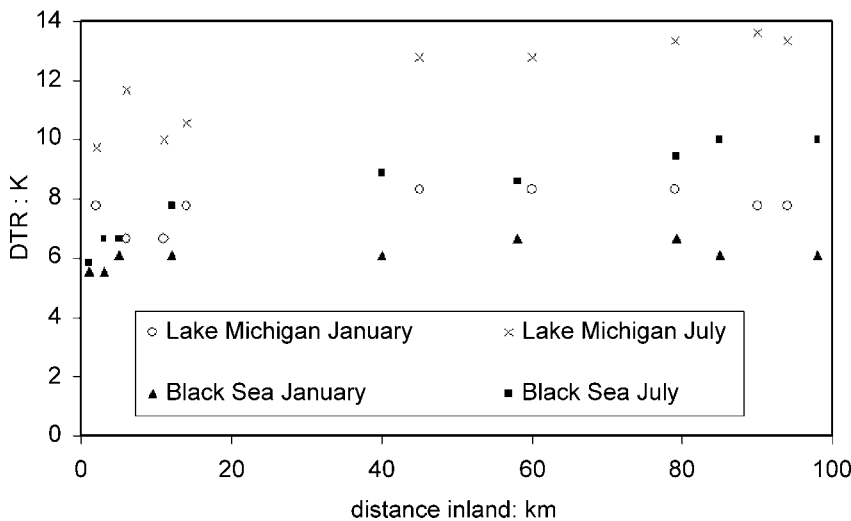


**Fig. 5.** The variation of the DTR in July and in January, as a function of distance eastward from the eastern shores of Lake Michigan (for places between 42.6–44.0° N) and the Black Sea (for places between 42.3–44.7° N) (ISMCS data)

**Table 1.** Mean DTR at various westbound distances from the western shore of Lake Michigan, at a latitude of  $40^{\circ} \text{N} \pm 0.5^{\circ}$ . Each distance group comprises 4 stations (source: ISMCS)

Distance	0–25 km	25–75 km	75–150 km
January	8.5	9.7	10.6
July	10.8	13.4	14.6

the near-shore DTR is depressed by about 2 K in winter and nearly 4 K in summer, compared to places 75–150 km further west (Table 1). This reduction is slightly higher than that observed east of Lake Michigan, where other lakes mainly further east may have some influence on the regional weather and therefore the DTR (Sousounis and Fritsch, 1994).

Relevant evidence also comes from Muynak, until the 1960's a fishing village on the southern shore of the Aral Sea. Between 1960 and 1992 the Aral Sea shrunk from 67,400 to 33,300 km<sup>2</sup>, and its southern shore moved north by about 100 km. During that period the DTR at Muynak increased by 3.3 K (Macleod and Mayhew, 1999, p. 313).

#### 4.2 Explanations

The reduction of DTR near the coast is partly explained by sea breezes. They commonly blow inland from Australia's east coast in summer, for example, but are absent when the ocean is relatively warm, off France in winter for instance. A sea breeze dynamically behaves like a density current, whose speed is proportional to the square root of its temperature deficit (Simpson and Britter, 1980). Therefore the strength and inland penetration of a sea breeze are larger where the difference between inland temperature and coastal sea surface temperature is larger. The wedge of cool marine air may continue to propagate inland in the late afternoon even as inland temperatures fall (e.g. Clarke, 1965), but the DTR will be lowered only if the sea breeze front forestalls the normally warmest time of the day, about 3 pm local time (LG97, p. 299). A typical sea breeze arises around 10 am and its forward boundary (the 'sea-breeze front') advances at no more than 15 km/h (Simpson, 1994). The maximum speed in Europe is about 9 km/h, and typical speeds observed at

Sydney were 6 km/h (Linacre and Barrero, 1974). So sea breezes can reduce the DTR only within at most 75 km of the shore (i.e.  $5 \text{ h} \times 15 \text{ km/h}$ ), and their impact on the DTR is largest near the coast.

The sea breeze penetrates less far or does not develop at all under less favourable conditions, e.g. under cloudy skies or when an offshore gradient wind blows. The fringe width is reduced also by coastal mountains where the cool marine air is capped by a subsidence inversion, e.g. along much of the California and Namibian coasts. In this case, the sea breeze is unable to rise over the terrain. But the sea breeze may combine with the anabatic mountain circulation, if the marine boundary layer is not capped (Abbs and Physick, 1992). Sea breezes are strongest and most frequent around  $10\text{--}30^{\circ}$ , because the daytime inland temperatures are high (Fig. 1) and prevailing winds weak. Sea breezes at middle and high latitudes occur only in the warm season, and they are weaker and less regular. The near-coast DTR should not be affected significantly by land breezes, which propagate offshore.

Similarly, lake breezes occur near the shore of large lakes, and may explain the observed DTR reduction within about 25 km from Lake Michigan's shore (Fig. 5, Table 1). Lake breezes are less common and remain more confined to the shoreline, compared with typical sea breezes (Estoque, 1981).

Observations in eastern Australia (Fig. 4) indicate that the coastal fringe, in which the DTR is reduced, is wider than 75 km in summer. Moreover sea breezes are rare in winter along the Australian east coast, yet the DTR is still reduced along the coast, albeit less than in summer. These observations suggest that other factors influence the DTR in the coastal fringe. Two factors are proposed, the variation of cloudiness with distance from shore, and onshore advection.

Firstly, clouds are more common in the coastal area of eastern Australia than west of the Dividing Range, as will be shown in Section 5. Secondly, prevailing onshore flow may reduce the DTR, through cold air advection at day and warm air advection at night. The change in sign of the thermal advection is due to a reversal in near-surface air temperature gradient across the coast. Marine air advected onshore gradually

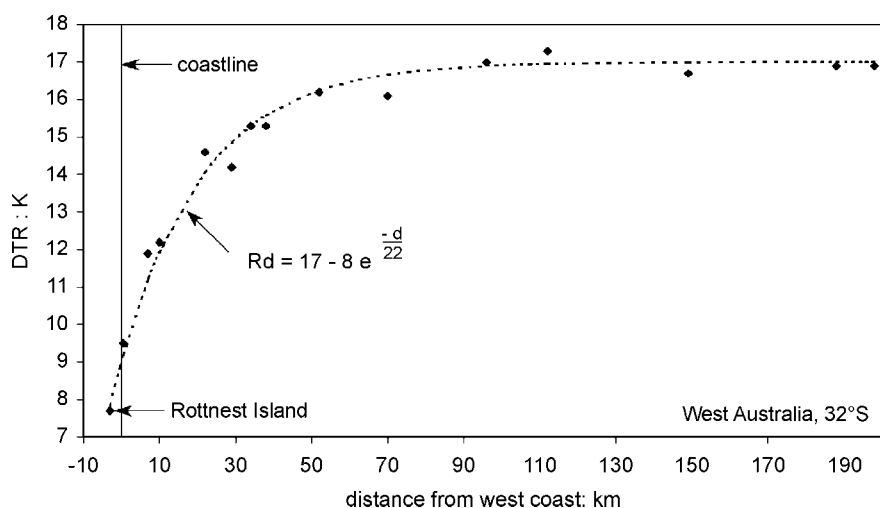


**Fig. 6.** Variation of January DTR with distance  $d$  (km) from Australia's west coast between 31.5–32.5° S (data from the Australian Bureau of Meteorology, at <http://www.bom.gov.au>)

adjusts to land surface conditions. Indeed, easterly flow prevails along Australia's east coast in summer.

Offshore flow and clear skies prevail on Australia's west coast around Perth in summer. Here the coastal fringe of reduced DTR values is only about 50 km wide (Fig. 6). Further inland the DTR is quite uniform around 17 K. The DTR 'deficit' is remarkably close to an exponential decay function, being about 8 K near the coast, and dropping off to 4 K at 15 km inland. This deficit can only be explained by sea breezes, which are common near Australia's southwest coast and occasionally penetrate far inland (Clarke, 1955). These observations imply that the air-conditioning effect of sea breezes (known around Perth as 'doctors') halves at each 15 km increment from shore. Inland DTR reductions exceeding this exponential decay must be due to onshore flow and variations in cloudiness.

#### 4.3 DTR variations further inland

The DTR may decrease gradually inland of the sea-breeze fringe, or more rapidly, depending on the prevailing airflow and topographic barriers. This is illustrated by contrasting the DTR change eastward across Eurasia and North America at 46° N (Fig. 7). The European DTR is about 6 K (11 K) in winter (summer), with little variation with distance from the Atlantic Ocean. It is reduced near the northern shores of the Adriatic and Black Seas, as well as in the Alps, and it is about 2 K larger at places at least 100 km from any coast. Further east at 46° N, east of

the Caspian Sea, the annual-mean DTR rises from 10 K at 4,000 km from the Atlantic Ocean to about 15 K at 8,000 km.

The DTR increases more rapidly east the Pacific Ocean (Fig. 7). The DTR values near the Pacific coast are similar to those in France, but they are 2–5 K higher between the coastal mountains and the Cascades in the summer. Both summer and winter values of DTR east of the Cascades are much higher than in Europe, at the same distance inland: the winter (summer) DTR is about 12 K (20 K) in the intra-mountain zone. This more rapid eastward increase of DTR, and the decrease of DTR east of the Rockies, is consistent with the low relative humidity in the intra-mountain zone, especially in summer (Section 5).

The impact of a topographic barrier on DTR is illustrated further by comparing the climate at Yakima, on the inland side of the Cascade Mountains at 230 km from the Pacific coast, to that at Lyon (France), located at approximately the same latitude, elevation and distance inland from the coast. Yakima has an annual-mean DTR of 15.2 K, which is 7.5 K larger than that of Lyon (based on the ISMCS). The prevailing wind is westerly in both Lyon and Yakima, and the mean wind speed is similar (9 vs 8 kts). But the average relative humidity is higher in Lyon (75% vs 57%), implying a higher probability of cloudy skies (4.7 oktas vs 3.8 oktas), especially at low levels. The relatively clear skies in Yakima are due to the Cascade Mountain range, aligned with the coast. These mountains shelter Yakima from marine airmasses.

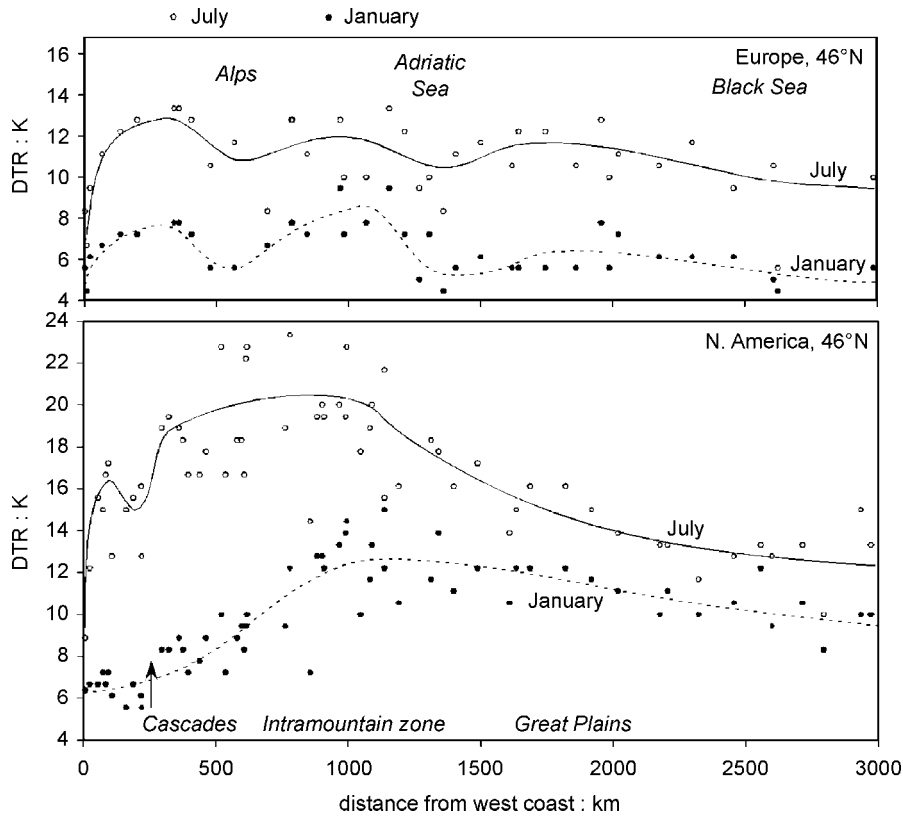


**Fig. 7.** The variation of the DTR in July and in January, as a function of distance eastward from the west coast of Europe (top) and North America (bottom) (ISMCS data). All stations are between 45.5 and 46.5° N. The solid (dashed) lines are subjective interpolations for July (January)

In summary, the observed variation of DTR further inland suggests a need to further explore the relationship between DTR and humidity or cloudiness.

## 5. Atmospheric moisture

### 5.1 Cloudiness, humidity and the DTR: a global perspective

The global distribution of annual-mean low-level cloud amount on land (Fig. 8) compares well with that of the DTR (Fig. 1). For instance low-level clouds are very rare in the Sahara, where the DTR is large. In the Congo and especially the Amazon Basin, low-level clouds are common and the DTR is low. There are two notable exceptions: cloud cover of 80% or more is reported in southeast China, while the DTR there is not correspondingly low. And in Siberia and in the Canadian Great Plains the low-level cloudiness is at most 40%, yet the DTR is small, less than 6 K. The latter anomaly is explained by the high latitude (Section 3).

The annual-mean surface relative humidity (RH) (Fig. 9) is directly related to low-level

cloudiness (Fig. 8), and therefore also correlates well with DTR (Fig. 1). The RH shown in Fig. 9 is not the average of instantaneous RH values but rather the RH computed from the annual-mean temperature and dewpoint values (Peixoto and Oort, 1996). The annual-mean RH in the central Sahara is less than 20%, lower than in Australia's interior for instance, consistent with the higher DTR in the Sahara than in Australia (Fig. 1).

The global distributions of DTR (Fig. 1), low-level cloud cover (Fig. 8), and RH (Fig. 9) suggest a good relationship between these variables. For instance, L92 (p. 80) reports the following linear regression for the monthly-mean DTR  $R_d$  (K), based on 357 locations worldwide:

$$R_d = 11.2 - 0.634 C + 0.355(T - T_d) - 0.04 T + 1.06 h \quad (2)$$

where  $h$  is the station elevation (km),  $C$  the monthly-mean amount of cloud (oktas) at any level, and  $T$  and  $T_d$  are the monthly-mean temperature and dewpoint (°C). Another empirical relationship between DTR and daily-mean dewpoint depression ( $T - T_d$ ) is given in Appendix A. The latter expression ignores cloudiness and

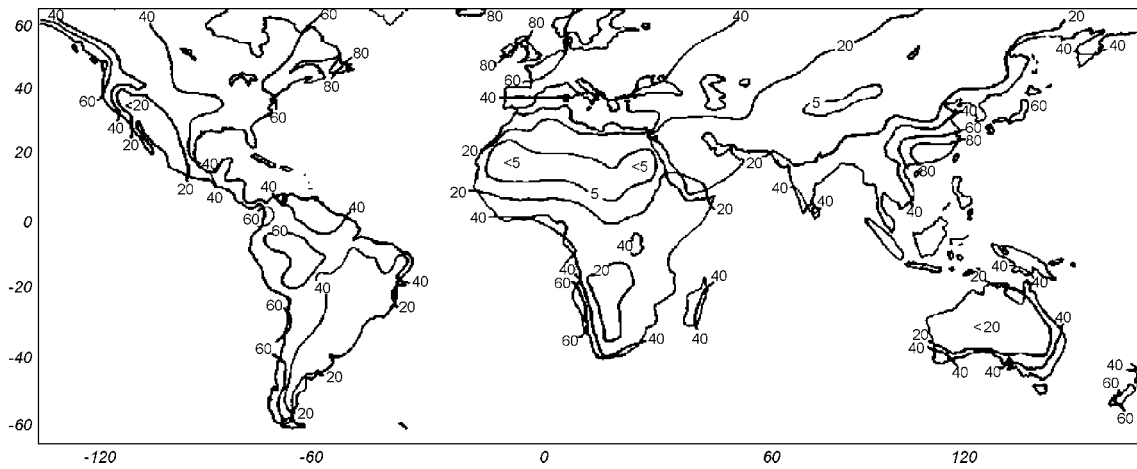


**Fig. 8.** Global distribution of the annual-mean low-level cloud amount (%) between 65°N–65°S, based on 11 years (1971–’81) of station observations. The contours are derived from data in Warren et al. (1986), who analysed cloud reports in 5° × 5° grid boxes. Low-level clouds include stratus, stratocumulus, cumulus, nimbostratus, and fog

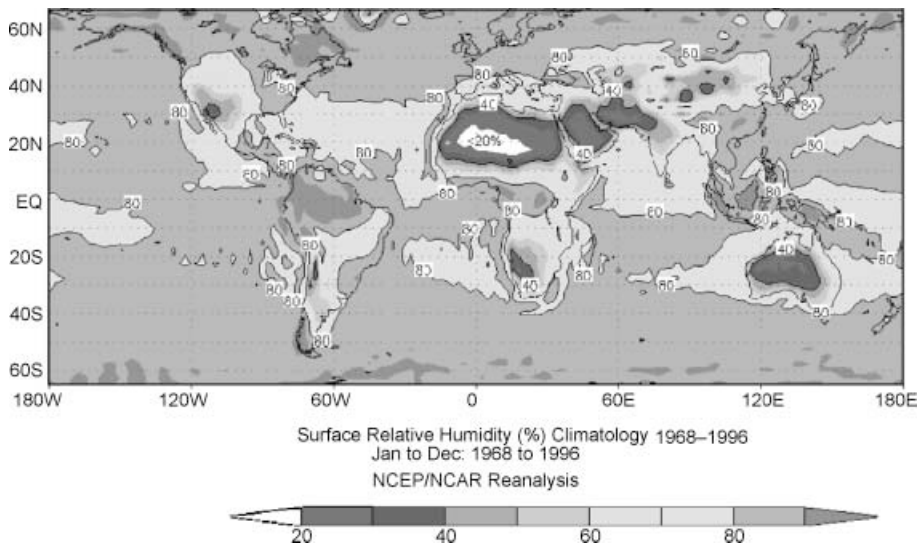


**Fig 9.** Global distribution of the annual-mean surface relative humidity between 65°N–65°S (Source: NNGR)

station elevation, yet it is more accurate than Eq. 2, at least for 60 stations in the USA around 46°N (Appendix A). This demonstrates that the DTR can be estimated with reasonable accuracy by a surface humidity variable alone, for instance the dewpoint depression, plus mean temperature.

### 5.2 Explanation

Clouds block the incoming solar radiation and reduce the net longwave radiation lost at the surface, implying a reduced DTR (e.g. McNider et al., 1995). Low clouds generally have a higher albedo and, more importantly, a higher base temperature, therefore they are more effective in

reducing the DTR at the surface and at screen level. The base temperature of stratus clouds imposes a radiative constraint on the minimum temperature at the ground. Mid- and high-level clouds are usually dynamically decoupled from the boundary layer, so their presence is largely independent of the surface conditions. At the same time their impact on the surface energy balance, and hence on the DTR, is smaller.

The presence of shallow clouds, such as cumulus humilis, stratocumulus or stratus, is linked to the dewpoint depression measured at screen level, through mechanical or buoyant mixing in the boundary layer, as explained in Appendix A. Therefore the relationship between DTR and

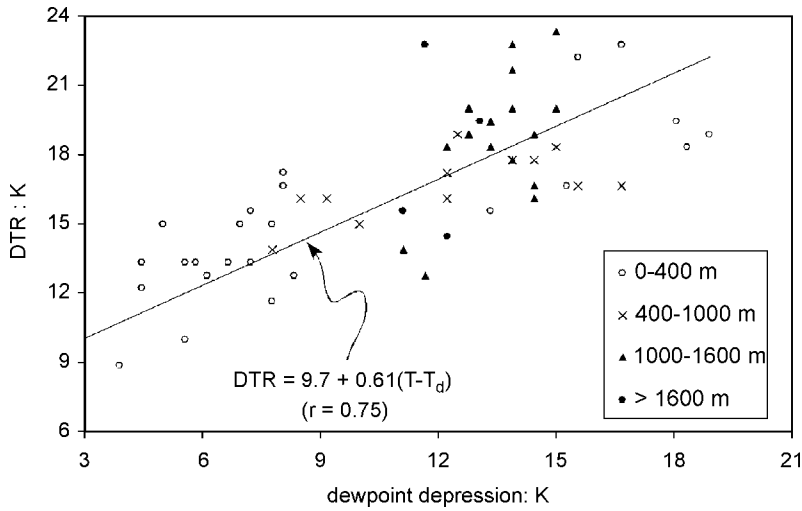


**Fig. 10.** The relation between July-mean DTR and dewpoint depression ( $T - T_d$ ) at 60 places in the western continental USA (west of  $95^\circ$  W). The dewpoint depression is the difference between the monthly-mean values of temperature and dewpoint. 'r' is the correlation coefficient. The places are stratified by elevation (ISMCS data)

dewpoint depression ( $T - T_d$ ), as in Eqs. 2 and A3, is not surprising.

### 5.3 Cloudiness, humidity and the DTR

The relation of DTR with dewpoint depression and with cloudiness is examined further for 60 places in the western USA. The correlation coefficient between the July-mean DTR and the dewpoint depression (Fig. 10) is 0.75, and that between the July-mean DTR and the total cloudiness (Fig. 11) is  $-0.70$ . In January (not shown) these figures are 0.62 and  $-0.49$  respectively. A more comprehensive station data analysis confirms that the correlation of DTR with total cloudiness is stronger in summer than in winter in N. America and Eurasia (Dai et al.,

1999). The reason is that in summer most clouds are rooted in the boundary layer. This applies to both shallow and deep cumulus clouds, and also to stratus clouds common in summer along the west coast of North America. In winter most clouds are associated with frontal disturbances. Much of that cloudiness results from uplift in the middle to upper troposphere, and may exist under dry surface conditions. The correlation of DTR with both dewpoint depression (Fig. 10) and cloudiness (Fig. 11) appears worse for the subset of more elevated places in the western interior, i.e. those above 1000 m. The likely reason for this is discussed in Section 6.

The observed decrease of DTR towards Australia's east coast (Fig. 4), attributed in Section 4 to sea breezes, can now be explained

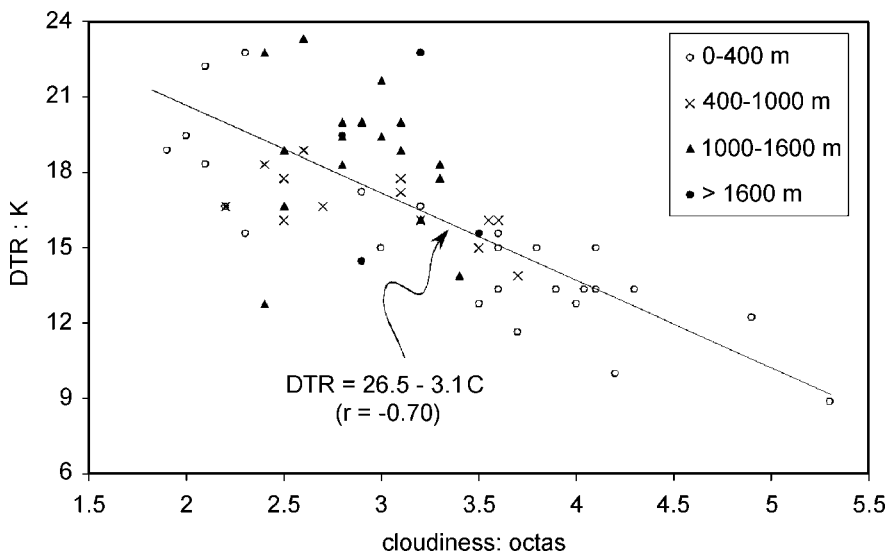


**Fig. 11.** As Fig. 10, but relating the July-mean DTR against cloudiness C at any level. The ISMCS reports the fraction of time with cloud-covered sky (8 oktas), broken clouds (6 oktas), scattered clouds (2 oktas), and clear sky (0 oktas). The cloudiness is calculated as the weighted average of these fractions

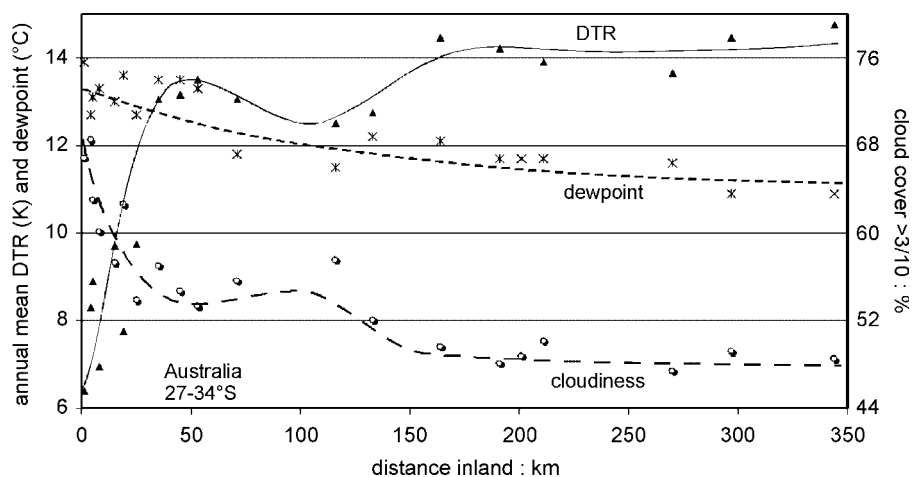


**Fig. 12.** The variation of annual-mean cloud cover, dewpoint, and DTR with distance from shore in eastern Australia between 27–34° S (ISMCS data). The stations are the same as those in Fig. 4. The cloud cover (expressed as the percentage of the time that it exceeds three tenths) and dewpoint data are based on twice-daily observations

by a second factor, i.e. the higher dewpoint and the more frequent occurrence of cloudy skies near the coast (Fig. 12). The dewpoint depression is not shown in Fig. 12, but it varies inversely to the dewpoint, because the mean temperature is about constant in this east–west transect (LG02). The rapid increase of DTR in the first 40 km from the shore is consistent with both the behaviour of sea breezes in this region, and with the rapid decrease of cloudiness. Beyond 150 km inland, the cloudiness becomes rather uniformly low, with less than 3 tenths of cloud cover during 50–55% of the time, and the DTR reaches a ceiling of about 14 K (LG97, p. 64). The distance of 150 km may be specific to the Australian east coast: it roughly coincides with the Dividing Range, which also corresponds to a large rainfall gradient.

Cloudiness and sea breezes act in a complementary way to reduce the near-shore DTR. On days when the coastal belt is cloudy, sea breezes are less likely because of inadequate surface heating. Sea breezes are more likely and stronger on clear days. In both cases the DTR will be reduced near the shore.

Differences in cloudiness do *not* explain the lower DTR near the shore of Lake Michigan, at least not in summer (Fig. 5). The DTR at near-shore stations in July is 2.7 K lower, on average, than that at inland locations (Table 2). This reduction is particularly remarkable in view of the *lower* cloudiness near the shore. Therefore it must be due to lake breezes and/or to onshore advection of air modified over the lake by the prevailing westerly wind. The occurrence of lake breezes is consistent with the lower cloudiness

**Table 2.** Average values of DTR, dewpoint, and cloudiness for the nine places near Lake Michigan shown in Fig. 5. Four places are within 15 km of the shore (“lakeshore”), and five places are between 45–95 km east of the shore (“inland”). The ISMCS reports the fractions of time with cloud-covered sky (8 oktas), broken clouds (6 oktas), scattered clouds (2 oktas), and clear sky (0 oktas). The cloudiness is calculated as the weighted average of these fractions

	Lakeshore	Inland
January		
DTR (K)	7.2	8.1
Dewpoint (°C)	–6.9	–7.8
Cloudiness (oktas)	6.5	6.2
July		
DTR (K)	10.5	13.2
Dewpoint (°C)	15.4	15.0
Cloudiness (oktas)	3.9	4.1

along the shore: cumulus clouds tend to build inland of the lake breeze. The higher afternoon RH near shore (5.3% higher, based on the July values in Table 2) is also consistent with this hypothesis. In fact lake breezes do frequent western Michigan in summer (Moroz, 1967). In January the lakeshore area is cloudier and receives more precipitation. This higher cloudiness does explain the reduced DTR near the shore, but this reduction is rather small, 0.9 K.

In summary, *the DTR is strongly correlated with low-level cloudiness*. This has been noted elsewhere (Dai et al., 1999; Durre and Wallace, 2001a). The variation of DTR with inland fetch is represented well by the low-level cloudiness, or by a measure of surface humidity such as dewpoint depression or RH. The inland penetration

of sea breezes, lake breezes, and the onshore advection of marine air all have one feature in common, that the RH increases towards the coast.

### 5.4 DTR and rainfall

The connections between, firstly, rainfall and cloud (LG97 p. 171), and, secondly, cloud and dewpoint depression (Appendix A), and, thirdly, dewpoint depression and DTR (Section 5.1), suggest relating rainfall to DTR directly. For instance, climate data from 70 places in the USA show that a daily rain amount of at least 1 mm in summer reduces the maximum temperature by about 3 K and increases the minimum by about 1.5 K, when compared to dry summer days (L92, p. 82). A relationship exists between monthly rainfall total  $P$  (mm) and monthly-mean DTR  $R_d$  (K) at 57 places in the USA, India and China, both in July and in January, i.e.  $[R_d = 13.5 - 2.0 \log P]$  (Fig. 13). The variation in rainfall amounts is expressed as a logarithm, reflecting the multiple-order-of-magnitude difference in  $P$  between dry and wet seasons. Independent analysis of January and July observations at 55 African places gives  $[R_d = 15.1 - 2.6 \log P]$ , which is similar. An intermediate expression may be taken as representative generally, as follows:

$$R_d = 14 - 2.3 \log P \quad (3)$$

It follows from this that a difference of DTR of merely 2.3 K means a ratio of monthly rainfalls of 10. That is confirmed also in Fig. 14 for Africa. The see-saw pattern of rainfall is a key factor in climate of Africa, which has well-defined belts of zenithal rain at low latitudes and a Mediterranean climate at high latitudes. The seasonal change of DTR is shown in Fig. 14, to eliminate the effects of elevation and proximity to sea. The DTR is greater in January than in July between the equator and the Tropic of Cancer at 23° N, especially at about 10° N, because July is wetter, even though the Sun is lower in the sky in January. And contrariwise in the south. This has been found to be the case at 46 out of 53 low-latitude places around the world, and true at all 30 places where the absolute difference between the January and

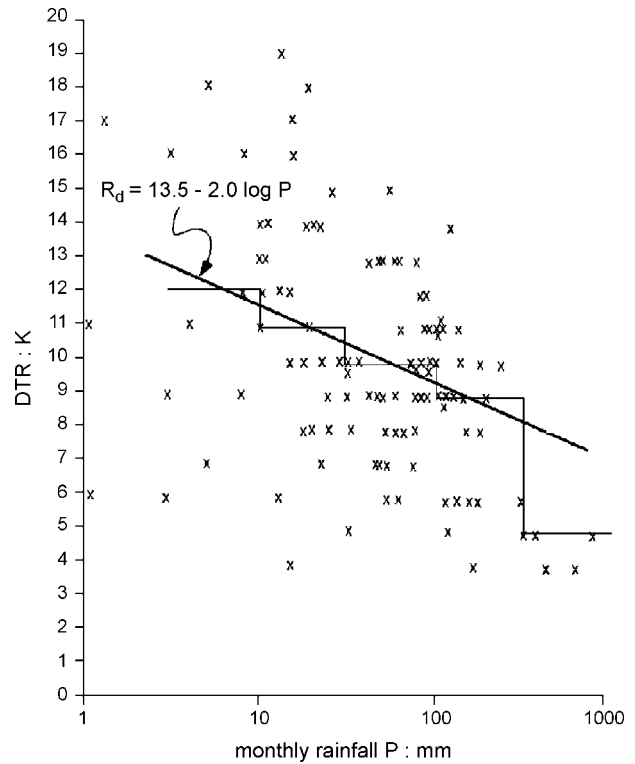


**Fig. 13.** The connection between the monthly-mean DTR and the monthly rainfall  $P$ , using 57 values from the USA, India and China listed in Pearce and Smith (1990). The horizontal lines show the median value for each band of rainfalls

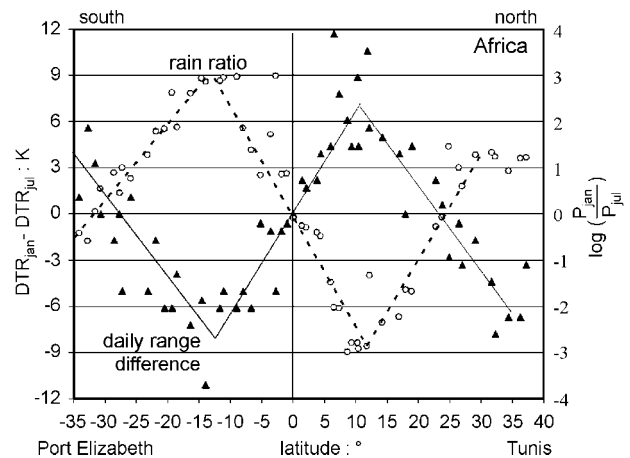


**Fig. 14.** The difference between the DTR in January and July (triangles), and the logarithm of the ratio of monthly total rainfalls in those months (open circles), along a transect through Africa at about 5–25° E, from Tunis to Port Elizabeth (ISMCS data)

July DTRs exceeds 2 K. The ratio of summer to winter rain is largest between 10–15°, where the seasonal range of DTR values is largest.

Note that Eq. 3 is not applicable to extremely dry places or seasons, and that it will overestimate the DTR in places experiencing much stratus but little rain, such as along some subtropical west coasts and at high latitudes. It also fails in many mid-latitude regions where the lower DTR in winter, compared to summer, is associated with a lower monthly rainfall. Hence the scatter in Fig. 13 is rather large.

The relationship between rainfall and DTR is not only explained by the association of rainfall with low-level clouds, but also by changes in the surface energy balance (Dai et al., 1999; Durre and Wallace, 2001b). Wet soils dispose of the net radiation more through evaporation than through sensible heat flux, implying a lower maximum screen temperature. Hence the maximum temperature is more sensitive to rainfall than the minimum temperature (L92, p. 82). Secondly, the higher conductivity and heat capacity of a moist soil decreases the soil DTR, and larger ground heat fluxes decrease the air DTR.

## 6. Topography

### 6.1 The effect of elevation on the DTR: observations

Equation 2, based on data worldwide, indicates an *increase* of DTR with elevation, of  $1 \text{ K km}^{-1}$ . This increase is not accounted for by the typical

increase of cloudiness and decrease of dewpoint depression in mountains, because these are separate variables in Eq. 2. Likewise, Fig. 3 in Linacre (1982), based on 139 places around the world, shows some increase of DTR with elevation, of about  $1.5 \text{ K km}^{-1}$ , though the scatter of points in that figure indicates that the DTR is likely determined by other factors. The DTR for the 60 places in the western USA shown in Fig. 10, with an elevation ranging between 4 and 2220 m, increases at  $1.6 \text{ K km}^{-1}$  ( $1.9 \text{ K km}^{-1}$ ) in January (July). Likewise, the annual-mean DTR in the central Andes is 2–6 K higher than at lower-elevation places both to the east and the west (LG97, p. 362). And on the island of Papua New Guinea/Irian Jaya the annual-mean DTR is about 4 K smaller near the coast than on the interior highlands at an elevation of about 1500 m (McAlpine et al., 1975; Allison and Bennett, 1976).

On the other hand, the DTR at 13 places in the Alps *decreases* at  $1.3 \text{ K km}^{-1}$ , more rapidly in July ( $2.1 \text{ K km}^{-1}$ ) than in January ( $0.4 \text{ K km}^{-1}$ ) (Fig. 15). The same DTR lapse rate is found between 200–1700 m altitude in the Western Carpathian mountains, located to the east of the Alps (Hess, 1968). [The annual temperature range also decreases with elevation in the Alps and the Western Carpathians (Geerts, 2002a).] Again a wide scatter of DTR values surrounds the linear trend in Fig. 15. In short, *elevation*

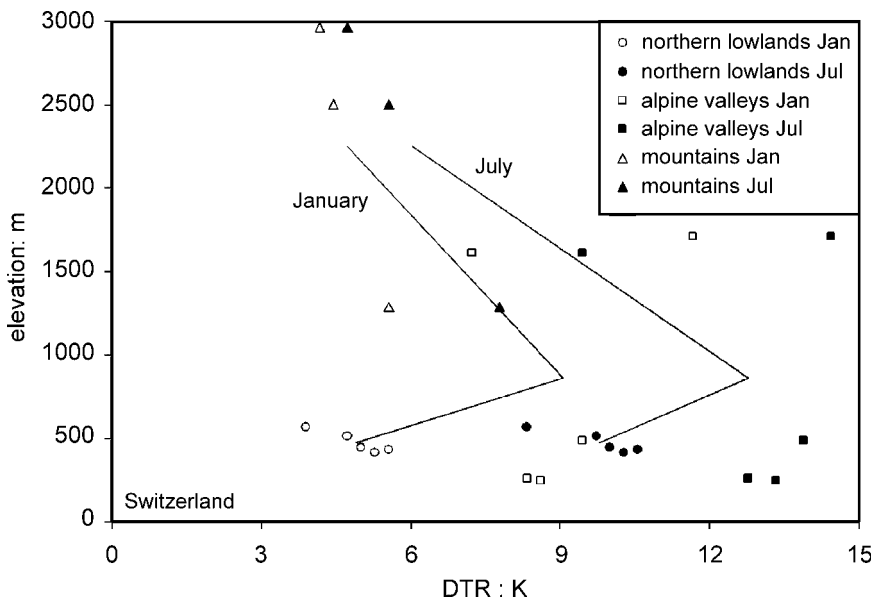


**Fig. 15.** Variation of monthly-mean DTR with elevation near the Alps in January and July. Eleven stations are in Switzerland and two places are just outside the Swiss border. They are classified in three types, northern lowlands (mostly broad valleys), alpine valleys, and mountaintops. The two lines connect the average DTRs and average elevations for each of these three types, for January and July respectively (ISMCS data).

*itself poorly correlates with DTR, and observations reveal opposing trends.* We now aim to explain these findings.

## 6.2 Explanation

Closer examination of Fig. 15 reveals that the average annual-mean DTR for five alpine valley locations is 10.9 K, which is 3.6 K higher than that for five places in the northern lowland of Switzerland. Some of these valley locations, such as Zermatt, are relatively high, above 1500 m. In fact on average the DTR increases with elevation between the northern lowlands and the alpine valleys, as can be seen in Fig. 15. On the other hand, the three stations located on mountaintops in Fig. 15 have an average annual-mean DTR of only 5.4 K, which is 5.5 K less than that at alpine valley locations. It is the small DTR at these mountaintop stations that explains the overall decrease of DTR with height observed in Switzerland. The mountaintop locations in Fig. 15 are not adjacent to the valley locations, nevertheless this strongly suggests that *local terrain shape affects DTR more than elevation.* The effect of terrain shape is explored further in Section 6.3. The reported increase of DTR with elevation at various places (Linacre, 1982) may be partly due to the common location of mountain settlements (and weather stations) in valleys.

The summer DTR is much higher than the winter DTR in alpine valleys (Fig. 15), presumably because in winter the Sun remains too low in the sky to warm the valleys effectively, while in summer the Alps experience less cloudiness. The small DTR on mountaintops is due to the ready mixing of near-surface air with free-tropospheric air, both in winter and summer, therefore the annual range of DTR is rather small on mountaintops, and the DTR decrease with elevation is more pronounced in summer.

## 6.3 Shape of the terrain

The propensity of valleys to have lower nocturnal temperature minima and larger DTRs compared to adjacent hills has long been known (e.g. Hann, 1903, p. 333; Geiger, 1965, p. 440). The following observations confirm its validity both in mid-latitudes and in the tropics.

- The DTR in two Alpine valleys (at about 1600 m elevation) is 6.0 K larger than at two mountaintop locations (at 2.5–3 km elevation) (Fig. 15). Average annual-mean wind speeds are 5.5 kts at these valley locations, compared to 17 kts on the mountaintops.
- A smaller DTR occurs on the hills in the Appalachians than in adjacent valleys (L92, p. 80).
- On the island of Papua New Guinea/Irian Jaya the DTR is 5–6 K smaller on the mountaintops (Mt Hagen and Mt Carstensz, respectively) than at surrounding highland villages, located in valleys at an elevation of about 1500 m (McAlpine et al., 1975; Allison and Bennett, 1976).
- The DTR decreases from about 15 K in the foothill valleys of the Himalayas to merely 2 K on an 8000 m mountain (quoted in Linacre, 1982).

The explanation is as follows: on calm, clear nights, cold air tends to drain from the higher terrain into valleys where it ponds. The result is a valley inversion, which vanishes during the daytime if the solar heating of the surface suffices. If this heating is not sufficient, which is common at higher latitudes in winter, the inversion may persist for days until winds associated with a frontal disturbance erode it. Inversions also develop on level land, but winds are generally lighter in valleys, facilitating the development of a nocturnal inversion even under less-than-ideal conditions. Therefore the DTR tends to be larger in valleys, as is the annual temperature range (Geerts 2002a).

A *terrain concavity factor* has been contrived in an earlier paper (Geerts 2002a) to quantify the effect of terrain shape on temperature range. For a valley the concavity is defined as the average depth of the valley divided by the distance between the peaks or ridges on opposite sides. So the concavity is zero for flat terrain. For a mountain location, the concavity is negative, i.e. the terrain is convex. There it is the height of the mountain divided by its typical width. In theory drainage flow is optimised under a certain concavity: on a very gentle slope gravitational acceleration of a wedge of cold air may not overcome friction (Stull, 1988, p. 534). On steep slopes adiabatic warming of drainage flow due

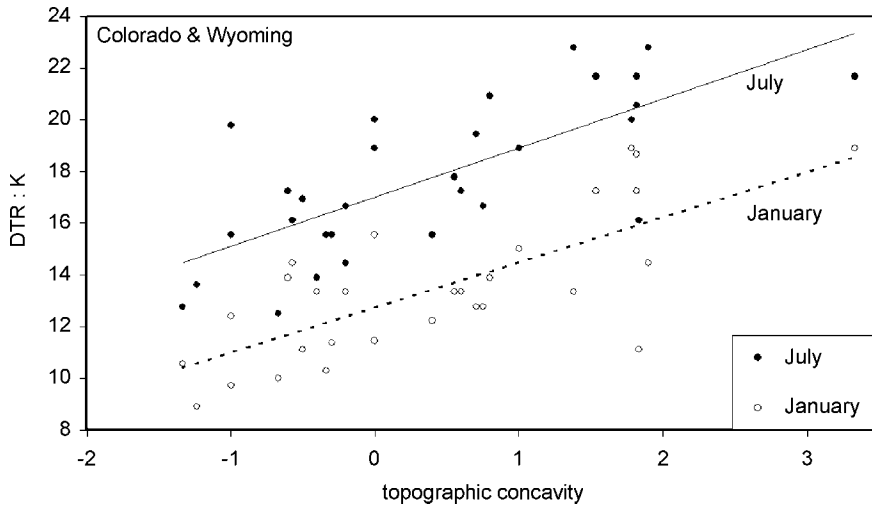


**Fig. 16.** The effect of the local terrain shape on the DTR, for 30 stations in Colorado and Wyoming, located between 37.5–44° N and 105–111° W. The data are obtained from the Western Regional Climate Center (<http://www.wrcc.sage.dri.edu>). The stations are at elevations ranging between 1429–3225 m. The solid (dashed) line is the linear regression for July (January)

to subsidence becomes important, and nocturnal radiative cooling in the valley is reduced by the smaller sky view factor (Oke, 1987).

The DTR is plotted as a function of concavity for 30 select stations in Colorado and Wyoming. This region is far inland and rather arid, explaining the large DTR, about 13 K in winter and 18 K in summer. There is more cloudiness towards the west in winter, and higher humidity towards the south in summer, but overall the region is rather uniform. Figure 16 shows a significant amount of scatter, due to variations in cloudiness, wind speed, and latitude, but nevertheless a clear correlation of DTR with concavity, both in January and July. The correlation coefficient for annual-mean DTR values is +0.75. The two lines shown in Fig. 16 suggest the following relationship between daily range  $R_d$  (K) and terrain concavity  $C_o$  (dimensionless):

$$R_d = R_{do} + 1.8 C_o \quad (4)$$

where  $R_{do}$  is the average DTR at neighbouring places on level terrain. Equation 4 applies both to monthly-mean and annual-mean values. The slope of the linear regressions, shown in Fig. 16, is 1.75 in January and 1.90 in July. This difference is small enough to be ignored in Eq. 4.

The validity of the linear relationship in Eq. 4 may be questioned for very ‘concave’ places,

which have a small sky view factor (Oke, 1987). At such places the surrounding canyon walls reduce the DTR. The most ‘concave’ place, Gunnison in Colorado, does not show a reduced DTR, suggesting that its concavity is less than the critical value.

For these select 30 stations the DTR actually decreases with elevation, by  $1.7 \text{ K km}^{-1}$ , whereas for the 60 stations in the western USA (shown in Fig. 10) the DTR increases with elevation, by about the same amount. The reason is that the 60 stations in the western USA lie in a heterogeneous region comprising both coastal stations with high cloudiness, and stations in the high desert.

The apparent increase of DTR with elevation in the western USA, as well as in the Andes (Linacre, 1982), can now be explained by the siting of highland stations in valleys, and by the aridity of the Rockies and the Andes compared to the lowland stations along the Pacific coast. Both the western and eastern sides of the Rockies between 30–50° N are cloudier, with mainly stratiform and cumuliform clouds respectively. The same applies to the Andes between 0–25° S (LG97, p. 68).

In summary, *scatter plots of DTR vs. elevation do not reveal an important mechanism controlling the DTR, i.e. the trapping of radiation inversions in valleys, enhanced by thermally forced circulations.*

## 7. Estimating the daily range of surface temperature

### 7.1 Justification

Table 3 summarizes the various DTR expressions that have been established or tested in this study. It should be cautioned that these relationships are based on data from specific stations, selected to illustrate a specific process, and therefore they may not apply generally. For instance stations were selected along a transect near Perth in January (Fig. 6), because DTR variations there can *only* be explained by sea breezes, since the prevailing offshore wind is replaced on most afternoons by an onshore wind at coastal places, the skies are generally clear (even at the coast), the terrain is nearly level. Similarly, to assess the effect of terrain concavity (Section 6.3), stations in valleys and on mountains were selected in an area that is otherwise rather homogenous. While the processes illustrated by the relationships in Table 3 are universal, the universal applicability of these equations has not been demonstrated.

We now seek to develop a simple relationship for the DTR that can be used globally to estimate

the DTR. We first demonstrate that the results reported earlier in this paper argue for a reasonably accurate, general relationship between DTR and RH plus mean temperature. The variation of DTR with latitude is somewhat regular (Fig. 2) and the error of Eq. 1 is rather small for the station data plotted in Fig. 3 (Table 3). However the latitudinal variation can be largely explained by variations in RH (Section 3), except at high latitudes where the decreased DTR can be modelled by mean temperature. The variation of DTR with distance from shore can be represented by the dewpoint depression (or RH), as discussed in Section 5.3. Low-level cloudiness is more relevant than cloudiness at any level, but it is available only for a small fraction of stations, unlike surface RH. The relationship between DTR and monthly rainfall (Section 5.4) also is represented well by the RH, as a higher water vapour content implies more rain, and wet soils imply a higher air humidity. Elevation has little direct effect on DTR (Section 6.1), yet it has been included in published equations such as Eq. 2; its significance, if any, can be represented by the mean temperature (LG02). The terrain concavity is

**Table 3.** Summary of the relationships of the monthly-mean daily range  $R_d$  (K) with other variables illustrated in this study. The symbols are: distance  $d$  (km), mean temperature  $T_m$  ( $^{\circ}\text{C}$ ), dewpoint  $T_d$  ( $^{\circ}\text{C}$ ), cloudiness  $C$  (oktas), precipitation  $P$  (mm/month),  $R_{do}$  the DTR over level terrain (K), and  $C_o$  the terrain concavity (dimensionless). ‘Summer’ (‘winter’) refers to the month of July in the north and January in the south (vice versa). The number in brackets below the mean absolute error (MAE) is the bias, which is zero for a regression developed here, and non-zero where a previously established relationship is tested. ‘ $r$ ’ is the correlation coefficient

Variable	Relationship	Number of places, location, relevant figure	Summer		Winter	
			MAE	$r$	MAE	$r$
Latitude	see Eq. 1	85, in the Americas, Europe & Africa (Fig. 3)	0.9 K (0)	0.91	1.5 K (0)	0.79
Distance from shore	$17 - 8 \exp(-d/22)$	15, in western Australia (Fig. 6)	0.4 K (0)	0.83		
Dewpoint depression	$9.7 + 0.61(T_m - T_d)$	60, in the western USA around $46^{\circ}\text{N}$ (Fig. 10)	1.7 K (0)	0.75	2.6 K (0)	0.62
Cloudiness	$26.5 - 3.1C$	60, in the western USA around $46^{\circ}\text{N}$ (Fig. 11)	1.8 K (0)	-0.70	3.4 K (0)	-0.49
Dewpoint & temperature	$\frac{T_m - T_d + 0.8 T_m - 0.018 T_m T_m - 5}{0.5 + 0.018 T_m}$	60, in the western USA around $46^{\circ}\text{N}$ (App. A)	2.3 K (0.6)	0.62*	2.7 K (0.7)	0.59*
Precipitation	$14 - 2.3 \log P$	112, from India, China, USA & Africa (Fig. 13)	1.9 K (-1.4)	0.78	3.1 K (-1.7)	0.68
Concavity	$R_{do} + 1.8 C_o$	30, in Colorado & Wyoming (Fig. 16)	1.6 K (0)	0.73	1.5 K (0)	0.74

\* Partial correlation coefficient for dewpoint depression

important (Fig. 16), but this variable is not readily available for any location, and it does not have a surrogate. So it must be excluded from the DTR estimation merely for a practical reason. Finally, Table 3 differentiates between summer and winter. This seasonal variation can be represented by the mean temperature.

The daily-mean RH may be a good proxy for the DTR (Fig. 9), but it is not a meaningful variable because the large daily RH range is due more to the DTR than to the daily range of vapour pressure (Linacre and Hobbs, 1977, p. 55). What distinguishes an arid place with a large DTR from a cloudy place with a small DTR is not the RH or dewpoint depression at night, but rather the low RH in the afternoon, i.e. the large value of  $(T_{\max} - T_d)$  (Appendix A). The *afternoon* or *daily-minimum* RH is most relevant, because of its relation to low-level cloudiness: the convectively-mixed boundary layer is best developed in the afternoon, whereas at night the surface conditions are often irrelevant to low-level cloud formation because of a shallow radiation inversion.

In summary, *an examination of the processes affecting the DTR suggests that a strong relationship should exist between DTR and daily-minimum relative humidity, plus daily-mean temperature.* This relationship, to be developed based on monthly-mean values, should be applicable in any season anywhere on land between  $65^\circ \text{N}$ – $65^\circ \text{S}$ .

## 7.2 Empirical estimation

January and July records were compiled for 142 ISMCS stations worldwide between  $65^\circ \text{N}$  and

$65^\circ \text{S}$ . The stations were selected to represent a broad range of RH values and temperatures. The ISMCS reports the RH twice daily. The afternoon RH,  $H_a$  (%), is defined as the RH value reported either at 3 pm or at 4 pm local time, depending on the station. So  $H_a$  is not necessarily the daily-minimum value, but it is usually close to it. The daily-mean temperature  $T_m$  ( $^\circ \text{C}$ ) is the average of the minimum and maximum values. The following relationship for monthly-mean DTR  $R_d$  (K) applies in any season:

$$R_d = 21.1 - 0.20 H_a - 0.03 T_m \quad (5)$$

The mean absolute error of Eq. 5 for 284 cases (142 stations, two months each) is 1.3 K. Inclusion of the latitude and/or the elevation of the station in the multiple regression does not appreciably improve the relationship. Separating Eq. 5 by season yields the following set of DTR estimates in summer  $R_{d,\text{SU}}$  and in winter  $R_{d,\text{WI}}$ :

$$R_{d,\text{SU}} = 23.2 - 0.23 H_a - 0.04 T_m \quad (6a)$$

$$R_{d,\text{WI}} = 19.6 - 0.18 H_a - 0.05 T_m \quad (6b)$$

[Note that ‘summer’ (‘winter’) refers to July in the northern hemisphere and to January in the south (vice versa)]. The mean absolute error of Eq. 6 is 1.2 K for the summer and 1.4 K for the winter, and the correlation coefficients between  $R_d$  and  $H_a$  are  $-0.94$  and  $-0.88$  respectively.

Figure 17 displays all data points leading to Eq. 5, as well as Eq. 5 itself for three values of mean temperature. Both Eqs. 5 and 6 confirm that the afternoon RH dominates the variation of DTR: an increase  $H_a$  by a mere 5% reduces

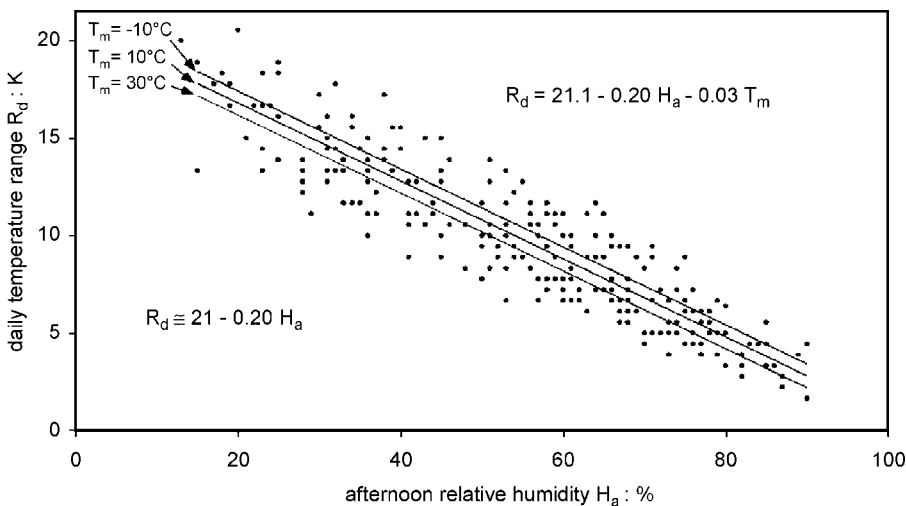


**Fig. 17.** Observed monthly-mean DTR plotted against afternoon RH for both January and July at 142 places worldwide (ISMCS data). The three lines represent Eq. 5, for different values of the mean temperature  $T_m$

the DTR by 1 K. This same change can also be accomplished by 20–30 K warming.

## 8. Discussion

The empirical estimation of DTR obtained in this paper is distinct from that for the annual-mean temperature (LG02) and the annual range (Geerts 2002a). The latter primarily used geographical information, such as latitude, elevation and distance from shore. Here, the DTR is estimated by means of climate variables, in an attempt to understand dominant atmospheric processes. A strong correlation has been found between DTR and the *afternoon* RH (Fig. 17). Clearly *atmospheric water vapour has no direct effect on DTR*, because as a greenhouse gas it increases both the minima and the maxima. But in the afternoon, when the boundary layer is best mixed, a high RH (or low dewpoint depression) implies a high probability of low-level clouds. *Low-level cloudiness reduces the DTR*, mainly through the damping of the maximum temperature (Dai et al., 1999).

The scatter of points around the regression lines in Fig. 17 is slightly larger at lower RH values, implying that the DTR is affected more by other factors under dry conditions. The next dominant factor is probably the shape of the terrain, in fact both valley and mountaintop locations were selected for Fig. 17. Most places worldwide are on relatively level terrain, for which the monthly-mean DTR, for any month of the year, can be estimated using Eq. 5.

The sensitivity of DTR mainly to afternoon RH  $H_a$  (%), apparent also in Fig. 17, suggests a further simplification of Eq. 5:

$$R_d = 21 - 0.20 H_a \quad (7)$$

The mean absolute error of Eq. 7 is 1.4 K, and the correlation coefficient between DTR and  $H_a$  is  $-0.92$ . Equation 7 implies that the observed global decrease of DTR of about 0.8 K per 100 years on land (Easterling et al. 1997) was accompanied by an increase in afternoon RH of about 4%. This implies a dewpoint increase of about 1.4 K in 100 years (Appendix B). Such increase in surface atmospheric water vapour content is consistent with observations in the USA (Gaffen and Ross, 1999), as well as with evidence for an

accelerated global hydrologic cycle (Dai et al., 1999).

## 9. Conclusions

This paper uses the global station climate record and gridded re-analysis data to describe and interpret spatial variations of the long-term average daily range of screen-level air temperatures (DTR). The main findings are:

- The DTR over land is larger in the subtropical belt ( $20^\circ$  to  $35^\circ$ ) than near the equator and in the mid-latitude belt. The highest values occur in the Sahara, about 18 K. The DTR is generally below 6 K poleward of  $45^\circ$ . At low latitudes the DTR is larger in winter, while at high latitudes it is higher in summer.
- The DTR near the coast is about half that at places further inland at latitudes near the Tropics. Reduced DTR values are found within 30–150 km from the coast. The reduction is explained by sea breezes, prevailing onshore winds, and/or more frequent low-level cloudiness nearer the coast. At higher latitudes the near-shore DTR reduction is smaller, and the more gradual increase of DTR inland is explained by dwindling atmospheric moisture over continents. The DTR is reduced also near large bodies of water, such as Lake Michigan in summer, but in a narrower belt. This reduction is explained by lake breezes.
- Inconsistent rates of change of DTR with elevation have been reported. Closer examination demonstrates that the changes with elevation can be explained mainly in terms of low-level cloudiness, and the shape of the local terrain. The DTR in valleys generally is 2–6 K more than on adjacent hills or mountaintops.
- The DTR is lower where the surface air humidity is higher, the low-level cloud cover larger, and the monthly rainfall amount larger. This applies both on a global and a regional scale. A most relevant variable is the afternoon relative humidity  $H_a$ , because it is coupled to low-level cloudiness through boundary-layer mixing.
- The monthly-mean DTR  $R_d$  (K) at any place on land between  $65^\circ$  N and  $65^\circ$  S can be estimated from the corresponding value of  $H_a$  (%), using the relationship  $R_d =$

$21 - 0.20 H_a$ , with an uncertainty of about 1.4 K. This relationship can also be used to understand the global DTR decrease observed in recent decades.

### Acknowledgements

Thanks are due to Edward Linacre (Australian National University) for inspiring this investigation and for his numerous critical reviews. Clive Hilliker drafted Fig. 13. Equation A.1.1 was derived by John Maindonald of the Australian National University.

### Appendix A. The DTR and the dewpoint temperature

Instantaneous daytime readings of the temperature  $T$  and the dewpoint  $T_d$  (both in °C) are a good measure of the height of the cloud base ( $H$  in km) for clouds resulting from buoyant or mechanical mixing within the boundary layer, i.e.  $H = (T - T_d)/8$  [since the lapse rate in the well-mixed boundary layer is 10 K/km, and the dewpoint lapse rate of an undiluted unsaturated air parcel equals 2 K/km]. Clearly if  $H$  exceeds the depth of the boundary layer, then there will be no cumulus or mixed-layer stratus. A convectively-mixed boundary layer is most common in the afternoon. If at this time the dewpoint depression is small, then  $H$  is small and (strato)cumulus clouds are more likely. The persistence of stratus clouds throughout the day is an indication that the dewpoint depression remains small.

Therefore the excess of the daily maximum temperature above the average dewpoint should be a good measure of low cloudiness and therefore the DTR. The mean temperature  $T_m$  and the DTR  $R_d$  allow derivation of the daily extremes,  $T_{\min}$  and  $T_{\max}$ , i.e.  $[T_m - 1/2 R_d]$  and  $[T_m + 1/2 R_d]$ , respectively. Then these can be used to estimate the dewpoint, as shown either diagrammatically (L92, p. 86) or in a table (LG97, p. 116), based on climatological *monthly-mean* values of daily extreme temperatures and dewpoint from 127 places around the world. Figures from the L92 diagram differ by 0.2 K on average (with a standard deviation of 3.8 K) from actual values of dewpoint determined at 46 other places.

Values from the table are now summarised in Eq. A1, as follows:

$$T_d = 0.38 T_{\max} - 0.018 T_{\max}^2 + 1.4 T_{\min} - 5 \quad (\text{A1})$$

Compared with values in the table, the standard error of the equation is 0.57 K. The equation means that a maximum of 25° C and a minimum of 15° C imply a dewpoint of 14° C, for instance. Similar equations have been derived, but not specified, for places in Spain (Castellvi et al., 1997). A large estimation error at any particular place or time indicates the influence of some additional local process (L92, p. 253).

Equation A1 can be used to obtain an expression for the *daily-mean dewpoint depression*  $[T_m - T_d]$ , units K] in terms of monthly averages of the mean temperature ( $T_m$ ) and the DTR  $R_d$

$$T_m - T_d = (0.018R_d - 0.8) T_m + 0.018 T_m^2 + 0.0045 R_d^2 + 0.5 R_d + 5 \quad (\text{A2})$$

Because the DTR is much less than 100 K, the  $R_d^2$  term in Eq. A2 can be omitted with an error less than 10% for a DTR of 11 K or less, in which case the DTR can be estimated as a function of the dewpoint depression and the mean temperature as follows:

$$R_d = (T_m - T_d + 0.8T_m - 0.018T_m^2 - 5)/(0.5 + 0.018T_m) \quad (\text{A3})$$

In this case the slope of the DTR increase, with increasing dewpoint depression, is 1:1 under warm conditions ( $T_m = 28^\circ \text{C}$ ) and 2:1 under cold conditions ( $T_m = 0^\circ \text{C}$ ). These slopes are much larger than that in Eq. 2, where it is 0.36:1. This small slope may be attributed to the partitioning of the effect of low-level cloudiness in two terms in Eq. 2, one for cloudiness  $C$  and one for surface humidity  $(T - T_d)$ . In Eq. A3 this effect is accounted for entirely by the surface humidity term.

Equation A3 was tested for 60 places in the USA around 46° N. The mean bias in estimated July DTR is 0.6 K, a slight overestimate, with a mean absolute error of 2.3 K. This proves that Eq. A3 is useful even for cases of high DTR, which exceeds 20 K in much of the western USA in July (Fig. 7). In January the mean bias is 0.7 K, with a mean absolute error of 2.7 K, for the same 60 places. Equation 2 does not do nearly as well for the same 60 places: the mean bias for the July (January) DTR is  $-3.5 \text{ K}$  ( $-2.0 \text{ K}$ ), an underestimate, with a mean absolute error of 5.2 K (4.1 K). The large underestimate in summer may be due to the lack of arid places in the data set leading to Eq. 2, resulting in too small a sensitivity of DTR to large values of dewpoint depression, as occur in the western USA in summer (Fig. 7).

These findings support the hypothesis that the DTR can be estimated with reasonable accuracy by a humidity variable (such as the dewpoint depression) and the mean temperature.

### Appendix B. Changes in DTR and dewpoint

Since the minimum relative humidity  $H_a$  generally occurs at the time of maximum daily temperature, Eq. 7 can be written as:

$$e_s\{T_d\} = e_s\{T_{\max}\}(21 - R_d)/20 \quad (\text{B1})$$

where  $e_s\{T\}$  is the saturation vapour pressure (hPa), which is a function of temperature  $T$ . Therefore small changes ( $\delta$ ) in dewpoint can be estimated from:

$$\delta e_s\{T_d\}/e_s\{T_d\} = \delta e_s\{T_{\max}\}/e_s\{T_{\max}\} - \delta R_d/(21 - R_d) \quad (\text{B2})$$

According to the Clausius-Clapeyron equation,

$$\delta e_s\{T\}/e_s\{T\} = L \delta T/(R_v T^2) \quad (\text{B3})$$

where  $L$  is the latent heat of vaporization ( $L = 2.5 \cdot 10^6 \text{ J kg}^{-1}$ ),  $R_v$  the gas constant for water vapour ( $R_v = 461 \text{ J K}^{-1} \text{ kg}^{-1}$ ), and  $T$  is any temperature (K). Plugging Eq. B3 into Eq. B2 yields the following expression for the change in dewpoint:

$$\delta T_d = \delta T_{\max}(T_d/T_{\max})^2 - \delta R_d(R_v/L)T_d^2/(21 - R_d) \quad (\text{B4})$$

Easterling et al. (1997) use global non-urban station data to show that the maximum temperature trend  $\delta T_{\max}$  has been  $+0.82 \text{ K/century}$  between 1950 and 1993, and the DTR trend  $\delta R_d - 0.79 \text{ K/century}$ . These tendencies yield a global increase in dewpoint of  $1.43 \text{ K/century}$ , according to Eq. B4. Interestingly, both the maximum temperature increase and the DTR decrease contribute about equally to this dewpoint increase.

## References

- Abbs DJ, Physick WL (1992) Sea-breeze observations and modelling: a review. *Aust Met Mag* 41: 7–19
- Allison I, Bennett J (1976) Climate and microclimate. In: Hope et al (eds) *The Equatorial Glaciers of New Guinea*. ■ Balkema, pp 61–80
- Castellvi F, Perez PJ, Stockle CO, Ibanez M (1997) Methods for estimating vapour pressure deficit on a regional scale, depending on data availability. *Agric Forest Meteor* 87: 243–252
- Clarke RH (1955) Some observations and comments on the sea breeze. *Austr Met Mag* 11: 47–68
- (1965) Horizontal mesoscale vortices in the atmosphere. *Austr Met Mag* 50: 1–25
- Crowe PR (1971) *Concepts in climatology*. ■ St. Martins's Press, 589 pp
- Dai A, Trenberth KE, Karl TR (1999) Effects of clouds, soil moisture, precipitation and water vapor on diurnal temperature range. *J Climate* 12: 2451–2473
- Deacon EL (1969) Physical processes near the surface of the earth. In: Flohn H (ed) *World survey of climatology*, Vol 2, Ch 2. ■ Elsevier, pp 39–104
- Dessens J, Bücher A (1995) Changes in minimum and maximum temperatures at the Pic du Midi in relation with humidity and cloudiness. *Atmos Res* 37: 147–162
- Durre I, Wallace JM (2001a) Factors influencing the cold-season diurnal temperature range in the United States. *J Climate* 14: 3263–3278
- , — (2001b) The warm season dip in diurnal temperature range over the Eastern United States. *J Climate* 14: 354–360
- Easterling DR, Horton B, Jones PD, Peterson TC, Karl TR, Parker DE, Salinger MJ, Razuvayev V, Plummer N, Jamason P, Folland CK (1997) Maximum and minimum temperature trends for the globe. *Science* 277: 364–367
- Estoque MA (1981) Further studies of a lake breeze. Part I: Observational study. *Mon Wea Rev* 109: 611–618
- Gaffen DJ, Ross RJ (1999) Climatology and trends of U.S. surface humidity and temperature. *J Climate* 12: 811–828
- Gallo KP, Easterling DR, Peterson TC (1996) The influence of land use/land cover on climatological values of the diurnal temperature range. *J Climate* 9: 2941–2944
- , Owen TW, Easterling DR, Jamason PF (1999) Temperature trends of the U.S. Historical Climatology Network based on satellite-designated land use/land cover. *J Climate* 12: 1344–1348
- Geerts B (2002a) Empirical estimation of the annual range of monthly mean temperatures. *Theor Appl Climatol* 73: ■–■
- Geerts B (2002b) On the effects of irrigation and urbanisation on the annual range of monthly-mean temperatures. *Theor Appl Climatol* 72: 157–163
- Geiger R (1965) *The climate near the ground*. Cambridge: Harvard University Press, 611 pp
- Hann J (1903) *Handbook of climatology*. ■ Macmillan, 437 pp
- Hansen J, Sato M, Ruedy R (1995) Long-term changes of the diurnal temperature cycle: implications about mechanisms of global change. *Atmos Res* 37: 175–209
- Hess M (1968) A new method of determining climatic conditions in mountain regions. *Geog Polonica* 13: 57–77
- Karl TR, Co-authors (1993) A new perspective on recent global warming: asymmetric trend of daily maximum and minimum temperature. *Bull Amer Meteor Soc* 74: 1007–1023
- Kukla G, Gavin J, Karl TR (1986) Urban warming. *J Climate Appl Meteor* 25: 1265–1270
- Landsberg HE (1981) *The urban climate*. *Int Geophys Series* 28: 275 pp
- Linacre ET (1982) Effect of altitude on the daily range of temperature. *J Climatol* 2: 375–382
- (1992) *Climate data and resources*. ■ Routledge, 366 pp
- , Barrero JA (1974) Surveys of surface winds in the Sydney region. *Proc. Internat. Geog. Union Regional Conf., & 8th New Zeal. Geog. Conf., Palmerston North (New Zeal. Geog. Soc.)* 247–260
- , Hobbs J (1977) *The Australian Climatic Environment*. ■ Jacaranda Wiley, 354 pp
- , Geerts B (1997) *Climate and Weather Explained*. ■ Routledge, 432 pp
- , — (2002) Estimating the annual mean screen temperature empirically. *Theor Appl Climatol* 71: 43–61
- McNider RT, Song JA, Kidder SQ (1995) Assimilation of GOES-derived solar insolation into a mesoscale model for studies of cloud shading effects. *Int J Remote Sens* 16: 2207–2231
- Macleod C, Mayhew B (1999) *Uzbekistan, the Golden Road to Samarkand*. ■ Odyssey, 328 pp
- McAlpine JR, Keig G, Short K (1975) *Climatic Tables for Papua New Guinea*. Tech paper No. 37, CSIRO Division of Land Use Research, 177 pp [Available from CSIRO Land and Water, GPO Box 1666, Canberra ACT 2601, Australia]
- Mearns LO, Giorgi F, McDaniel L, Shields C (1995) Analysis of variability and diurnal range of daily temperature in a nested regional climate model: comparison with observations and doubled CO<sub>2</sub> results. *Clim Dyn* 11: 193–209
- Moroz WJ (1967) A lake breeze on the eastern shore of Lake Michigan: observations and model. *J Atmos Sci* 24: 337–355
- Oke TR (1987) *Boundary Layer Climates*. London: Methuen & Co., 435 pp
- Pearce EA, Smith CG (1990) *The World Weather Guide*. Hutchinson, 480 pp
- Peixoto JP, Oort AH (1996) *The climatology of relative humidity in the atmosphere*. *J Climate* 9: 3443–3463
- Simpson JE (1994) *Sea Breezes and Local Winds*. Cambridge University Press, 234 pp

- , Britter RE (1980) A laboratory model of an atmospheric mesofront. *Quart J Roy Meteor Soc* 106: 485–500
- Sousounis PJ, Fritsch JM (1994) Lake-aggregate mesoscale disturbances. Part II: A case study of the effects on regional and synoptic-scale weather systems. *Bull Amer Meteor Soc* 75: 1793–1812
- Stull RB (1988) *An introduction to Boundary-Layer Meteorology*. Kluwer, 666 pp
- Warren SG, Hahn CG, London J, Chervin RM, Jenne RL (1986) Global distribution of total cloud and cloud type amounts over land. NCAR Tech. Note TN-273 & STR/DOE Tech. Rep. ER/60085-HI, 29 pp. + 200 maps [NTIS #DE87-00-6903]
- Watterson IG (1997) The diurnal cycle of surface air temperature in simulated present and doubled CO<sub>2</sub> climates. *Clim Dyn* 13: 533–545
- Author's address: Dr. Bart Geerts, Department of Atmospheric Sciences, University of Wyoming, Laramie WY 82071, USA (e-mail: geerts@uwyo.edu)

Dear Author,

The goal of our new, more rapid publication procedures is to publish your paper online as quickly as possible. The assigning of a DOI (digital object identifier) at this stage means that the work is fully citeable much earlier than has previously been the case. Please note that final pagination will be added only when articles have been assigned to a printed issue. With respect to the quality of figures in the electronic version, please note that the printed version will be of the usual high quality. For a list of all papers published online so far, please refer to the following web-site (your paper will be added to this list after final correction):

<http://link.springer.de/link/service/journals/00704/tocs.htm>



Instruction to printer	Mark	Examples	
		In the text	In the margin
Character to be corrected	/	Letter to be corrected	e /
Group of characters to be corrected	H	Letters to be corrected	ed H
Several identical characters to be corrected	/	Council for Commission	o ///
Differentiation of several errors in the same paragraph	1 F L J	There are many faults in this line	r / L m / i / a F
Character or word to be deleted	o	Commission and Parliament	o y o H
Character or word to be added	h	A word missing	is h
Superior character required	^	The Court's judgment.	(^) /
Omitted text to be added (see copy)	h	1. January 12. December	h (Out see copy)
Inferior character required	v	H <sub>2</sub> SO <sub>4</sub>	4 /
Change to italic		Ad infinitum	(ital.)
Change italic characters to roman	o	status quo	(rom.)
Change capitals to lower case	o	UNESCO	(l.c.)
Change to capitals or small capitals	= =	Robert Burns, AD 1759-96	(Caps.) (S.C.)
Change to bold face	~~~~~	This word needs emphasising!	(bold)
To be letter-spaced		<del>This line is crooked</del>	/
Correct horizontal alignment		<del>This line is crooked</del>	/
Text to be raised or lowered	∩ ∪	This line is uneven	∩ / ∪ /
Text to be aligned (to the left)	⌋	This text is to be aligned	⌋ /
Text to be aligned (to the right)	⌈	This text is to be aligned	⌈ /
Text to be centred	[ ]	This text is to be centred	[ ] /
Take back to previous line	] ]	This hyphen is unnecessary	] /
Text to run on (no new paragraph)	~	... line. No new paragraph here	~ /
Take forward to next line	[ ]	This hyphen is badly placed	[ /
Create new paragraph	⌋ ⌈	... line. A new paragraph should begin here	⌋ / ⌈ /
Close up	o o	A space is wrong here	o /
Equalise space	/	This spacing is very uneven	∩ /
Add space between words	z	A space is missing here	z # /
Reduce space between words	∩	These spaces are too big!	∩ /
Add space between lines	Y #	These lines are too close together	Y #
Reduce space between lines	↑	These lines are too far apart.	↑ /
Stet (let original text stand)	⋮	This text was corrected in error	⊙
Transpose characters	S	These letters are transposed	S /
Transpose words	∩	These words are transposed	∩ /
Transpose lines	∩	These lines are transposed	∩ /

NB: A correction made in the text must always have a corresponding mark in the margin, otherwise it may be overlooked when the corrections are made. The same marks should be used, where appropriate, by copy-editors marking up copy. Where instructional words are used in marginal marks, e.g. 'ital.', 'bold', etc., they must always be encircled to show that they are not to be printed.

